SHAPE OPTIMIZATION OF INLET HEADER OF MICRO-CHANNEL HEAT SINK USING SURROGATE MODEL COMBINED WITH GENETIC ALGORITHM

by

Huaishuang SHAO, Zongyi WANG, Min LIAO, Chao LI, Zhiyuan LIANG, and Qinxin ZHAO*

Key Laboratory of Thermo-Fluid Science and Engineering, Ministry of Education, Xi'an Jiaotong University, Xi'an, Shaanxi, China

Original scientific paper
https://doi.org/10.2298/TSCI221219074S

A lot of work has documented the significance of fluid-flow uniformity on the thermal-hydraulic performance of the micro-channel heat sink. The purpose of this work is to optimize the shape of inlet/outlet headers of a micro-channel heat sink to improve the flow distribution characteristics using the back propagation neural networks combined with the genetic algorithm as the surrogate model. The slanted edge of the inlet header is defined as the quadratic parabola instead of straight line. Meanwhile, the shape of the parabola is optimally designed for different flow rates. The 40 training sample points and six testing sample points on different geometry structures of inlet header are designed by the Latin hypercube sampling method. The 3-D CFD calculation is performed for all models. The objective function is defined as the non-uniformity of the fluid-flow. It is found that the prediction of the genetic algorithm back propagation for the fluid-flow distribution is capable of obtaining objective function values within the designed space. Through the optimizations, the non-uniformity of the optimal inlet header structure can be reduced by 52.43% to 33.17% for the inlet velocity of 0.05 m/s to 0.1 m/s, respectively, compared to that of the original design. The results demonstrate that the parabolic treatment for the slanted edge of the inlet header as well as structural optimization can greatly improve the flow uniformity of the micro-channel heat sink.

Key words: *shape optimization, micro-channel heat sink, flow characteristics, surrogate model, genetic algorithm*

Introduction

Micro-channel heat sink (MCHS) and micro-electromechanical systems (MEMS) have been widely used in aerospace engineering, military and nuclear energy, fuel cell systems, solar thermal collectors, piping systems, chemical technology and other fields [1-4]. Flow distribution is a key cog in MCHS designation, which has been documented in a vast literature. Flow maldistribution deteriorates the thermal-hydraulic characteristics of MCHS, as an example, the heat transfer performance will sharp degrade on account of the fluid-flow maldistribution.

Tuckerman *et al*. [5] proposed the concept of a microscopic channels firstly. The performance of the MCHS was tested and conducted with experiment. The results indicate

* Corresponding author, e-mail: zhaoqx@jtu.edu.cn

that the maximum heat flux of the MCHS can reach up to 7.9 MW/m^2, which reflects a high efficiency of heat dissipation. Dewan *et al*. [6] reviewed the triggers of flow maldistribution in the heat exchanger. A series of research work concerning experimental tests and numerical studies were carried out to analyze and improve flow characteristics. Bajura *et al*. [7] investigated the flow distribution of manifold analytically and experimentally. The dimensionless parameters that affect the flow distribution are discussed with the help of numerical model. Arie *et al*. [8] developed a hybrid method, which is able to evaluate the performance of MCHS with faster calculation speed. Joshua *et al*. [9] conducted the study on the optimization of flow distribution and pressure drops in *Z*-type configurations of fuel cells. The fluid-flow is assumed as a steady state to simplify the control equations of the discrete model, which would be solved by means of a constructed algorithm using FORTRAN 77 programming language. Meanwhile, a general and simple optimization method is also proposed. Midoux *et al*. [10] demonstrated a theoretical overview of the flow distribution within the manifolds, which includes parallel channels with *Z*-type and *U*-type configurations. The investigation results indicate that the diameters of the distributor and collector may have a significant impact on flow distribution, as shown in fig. 1.

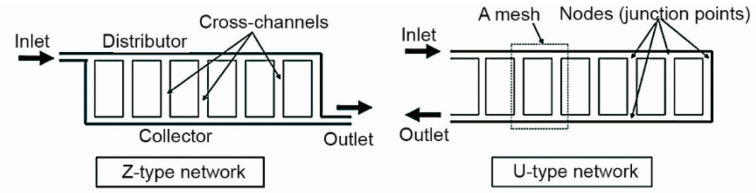

Figure 1. General configurations with six meshes and seven cross-channels [10]

The structural optimization on micro-channel flow and heat transfer characteristics have also been carried out and performed at the same time. Pan *et al*. [11] appended a series of reentrant cavities to micro-channels and comparatively investigated the performance of the heat exchanger with and without reentrant cavities. The numerical method of finite volume method (FVM) was adopted to solve the laminar developing flow. The results manifest that the heat exchangers with reentrant cavities perform better with an acceptable pressure drop increase. Solovitz [12] performed the numerical study on the 3-D geometry model with both constant channel aspect ratio and varying aspect ratio. It shows that the standard deviations of channel speeds varying below 3% at low Reynolds numbers. However, the flow asymmetry appears at higher speeds. Kumaran [13] studied the effects of header design on flow mal-distribution in a micro-channel heat sink by experimental and numerical methods. It is found that the manifold shape, manifold size and locations of inlet and outlet arrangements have a large effect on flow. The flow separation and recirculation bubbles occurring in the inlet manifold triggers the flow mal-distribution in the manifold systems. The *C*-type configuration outperforms a lot, while the *V*-type configuration performs the worst in flow distribution of channels. Sehgal *et al*. [14] conducted a series of investigation on the *U*-type, *S*-type, and *P*-type configurations pieces with two channel aspect ratios (4.72 and 7.57) and three plenum aspect ratios (2.5, 3.0, and 3.75). It is suggested that shrinking channel width might result in 126% to 165% increase in Nusselt number. Nevertheless, increasing in plenum length brings about just 18% to 26% increase in Nusselt number. Anbumeenakshi *et al*. [4] performed a detailed experimental investigation

to analyze the flow maldistribution in a micro-channel heat sink with three types of header shapes (rectangular, trapezoidal, and triangular) and two types of inlet configurations (vertical and inline flow inlet). It indicates that the performance in inline flow inlet configuration is relatively poor in terms of flow distribution ($200 \leq Re \leq 650$). Besides, it is found that the rectangular header at high flow rate gives a better performance.

In addition to the methods of numerical simulation or experimental verification mentioned above, optimization methods coupled with surrogate model have also been extensively practiced in the field of energy conversion and management. Koo *et al*. [15] investigated fluid-flow in printed circuit heat exchanger (PCHE). The Kriging and the radial basis neural networks (RBNN) are used as surrogate models and the objective function values acquired by the two surrogate models are compared. Shi *et al*. [16] acquired specific fluid-flow distribution of channels in a ceramic MCHS by means of the RBNN. The genetic algorithm (GA) is applied to search for the optimal point within the designed space. Wen *et al*. [17], Yang *et al*. [18], and Yildizeli *et al*. [19] investigated the fluid-flow and conjugate heat transfer in MCHS utilizing the non-dominated sorting genetic algorithm (NSGA-II) and the multi-objective genetic algorithm (MOGA). The optimal pareto front is obtained to provide a theoretical reference of flow uniformity and heat transfer for MCHS. Ge *et al*. [20] and Wang *et al*. [21] proposed a design criterion to reach the preference perform of the MCHS.

It can be seen from the previous research review that the current investigation on inlet header to uniform the fluid-flow of the MCHS mainly focuses on the shape of rectangle, trapezoid and triangle. The slanted edge of the inlet header is generally in the form of straight line. It has a limited effect on adjusting the local flow field inside the inlet header. In this work, the concept of parabolic slanted edge instead of straight line for the inlet header is proposed and the effect on the flow distribution of the MCHS is studied based on the rectangular inlet header. Meanwhile, the shape optimization of the quadratic parabola has also been conducted in detail under the condition of different inlet velocities.

Geometry model and problem description

A geometry model of the MCHS is shown in fig. 2. In this heat exchanger, the cross-sectional size of each micro-channel is 0.5 mm × 0.5 mm. The distance between adjacent micro-channels is 0.5 mm. The other parameters of the MCHS in detail have been listed in tab. 1. The water enters from the inlet header and flows into 20 micro-channels. It finally flows out through the outlet header. Affected by the shape of inlet header, it is more inclined to cause the uneven flow distribution in the micro-channels. The length of the slanted edge for the rectangular inlet header is w_h, as shown in fig. 2. In this work, the parabolic shape for the slanted edge of the inlet header is studied through parametric optimization. The length x_1 of the bottom edge for the rectangular inlet header remains constant. The length x_2 of the top edge for the rectangular inlet header varies between 0 mm and 4 mm. In addition, the curvature of the parabola can be changed by changing the coefficients of the quadratic parabola. This part will be described in detail in the next section.

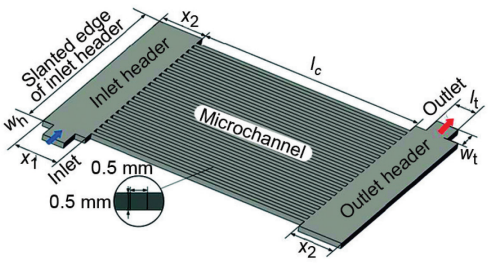

Figure 2. Schematic of the original MCHS with the rectangular inlet header

Table 1. Structure size of the MCHS

Term	Parameters of geometry						
	w_h	x_1	x_2	l_c	l_t	w_t	D_h
Value [mm]	21.5	4	[0,4]	20	2	2	0.5

In the 3-D numerical simulation, the velocity boundary is used for the inlet (0.05 m/s, 0.06 m/s, 0.07 m/s, 0.08 m/s, 0.09 m/s, and 0.1 m/s) and the pressure boundary is used for the outlet (0 Pa). Other surfaces are set as the wall with no slip condition. Meanwhile, some assumptions are as follows.

– The water flow is in steady-state and incompressible.
– The water exhibits constant thermos-physical properties.
– The influence of gravity is negligible.

The Reynolds number in the micro-channel is calculated:

$$\mathrm{Re} = \frac{UD_h}{\nu} \tag{1}$$

where U [ms^{-1}] is the mean velocity of the water in one micro-channel, ν [m^{2}s^{-1}] – the kinematic viscosity of the water, and D_h [m] – the hydraulic diameter of one micro-channel, and can be calculated by:

$$D_h = \frac{4A_c}{P} \tag{2}$$

where A_c [m^2] is the cross-sectional area of one micro-channel and P [m] – the channel-wetted perimeter. Based on these assumptions, the constitutive equations of the fluid-flow within the MCHS can be described as follows.

Continuity equation:

$$\frac{\partial \rho}{\partial t} + \frac{\partial (\rho u_i)}{\partial x_i} = 0 \tag{3}$$

Momentum equation:

$$\frac{\partial}{\partial t}(\rho u_i) + \frac{\partial}{\partial x_i}(\rho u_i u_j) = -\frac{\partial p}{\partial x_i} + \frac{\partial}{\partial x_j}\left[\mu\left(\frac{\partial u_i}{\partial x_j} + \frac{\partial u_j}{\partial x_i}\right) - \frac{2}{3}\delta_{ij}\frac{\partial u_j}{\partial x_i}\right] +$$

$$+ \frac{\partial}{\partial x_j}(-\rho u_i' u_j') + \rho g + F_a \tag{4}$$

The shear-stress transport (SST) *k-ω* model is selected to simulate turbulent flow, and it can also simulate laminar flow by set the region as *laminar zone* in ANSYS FLUENT. It has the advantages on the robust and accurate formulation both in the near-wall region and in the far field, which can simulate the sudden expansion, diffusion and backflow occurring in the inlet header and outlet header accurately. For the steady flow, the SST *k-ω* model can be presented:

$$\frac{\partial}{\partial x_i}(\rho k u_i) = \frac{\partial}{\partial x_j}\left[\left(\mu + \frac{\mu_t}{\sigma_k}\right)\frac{\partial k}{\partial x_j}\right] + \mu_t S^2 - \rho\beta^* \omega^2 \tag{5}$$

$$\frac{\partial}{\partial x_j}(\rho\omega u_j) = \frac{\partial}{\partial x_j}\left[\left(\mu + \frac{\mu_t}{\sigma_\omega}\right)\frac{\partial \omega}{\partial x_j}\right] + \frac{\alpha}{v_t}\mu_t S^2 - \rho\beta\omega^2 + 2(1-F_1)\rho\frac{1}{\omega\sigma_{\omega,2}}\frac{\partial k}{\partial x_j}\frac{\partial \omega}{\partial x_j} \quad (6)$$

where S is the mean rate-of-strain tensor, μ_t – the turbulent viscosity, σ_k and σ_ω – the turbulent Prandtl numbers for k and ω, respectively, y – the distance to the next surface and D_ω^+ – the positive portion of the cross-diffusion term. The corresponding thermos-physical properties are listed in tab. 2 and the constant values in this model are:

$$\sigma_{k,1} = 1.176, \quad \sigma_{\omega,1} = 2.0, \quad \sigma_{k,2} = 1.0, \quad \sigma_{\omega,2} = 1.168, \quad \sigma_1 = 0.31,$$
$$\beta_{i,1} = 0.075, \quad \beta_{i,2} = 0.0828$$

Table 2. Thermo-physical properties of water

Term	ρ [kgm^{-3}]	μ [Nsm^{-2}]	ν [m^{2}s^{-1}]
Value	998.2	$1.003 \cdot 10^{-3}$	$1.005 \cdot 10^{-6}$

For this geometry, the unstructured and hexahedral mesh is generated. For grid-independent verification, four sets of grids with different number of grids are generated by encrypting the micro-channels to different degrees. Grid independent verification of the rectangular header model was conducted at an inlet flow rate of 0.05 m/s. Four different grid systems with the number of grids ranging from $1.21 \cdot 10^6$ to $3.55 \cdot 10^6$ were tested. As the number of grids increases, the third grid system with grid number $2.73 \cdot 10^6$ does not differ much from $3.55 \cdot 10^6$, which shows in tab. 3. After weighting the computational accuracy and resource consumption, the third grid is adopted to the calculation, which is shown in fig. 3. Meanwhile, the generation method of the third grid system is applied to all the other geometry models.

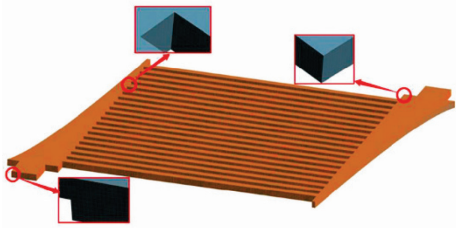

Figure 3. The diagram of grid

Table 3. Grid independence verification at an inlet flow rate of 0.05 m/s

Term	Number of grids	Outlet velocity of Channel 1 [ms^{-1}]	Error [%]	Outlet velocity of Channel 9	Error [%]
Grid 1	1210000	0.01219	1.89	0.00902	1.22
Grid 2	1820000	0.01196	2.76	0.00913	0.99
Grid 3	2730000	0.01163	0.60	0.00922	0.76
Grid 4	3550000	0.01156	–	0.00929	–

The descripted numerical simualtion model has also been verified with the experimental correlation of Mahshid Mohammadi *et al.* [22] for the rectangular micro-channel [23]. The experimental correlation are:

$$f\mathrm{Re} = 24(1 - 1.3553\alpha + 1.9467\alpha^2 - 1.7012\alpha^3 + 0.9564\alpha^4 - 0.2537\alpha^5) \quad (7)$$

$$\Delta P = 2 f \rho \frac{L}{D_h} U^2 \tag{8}$$

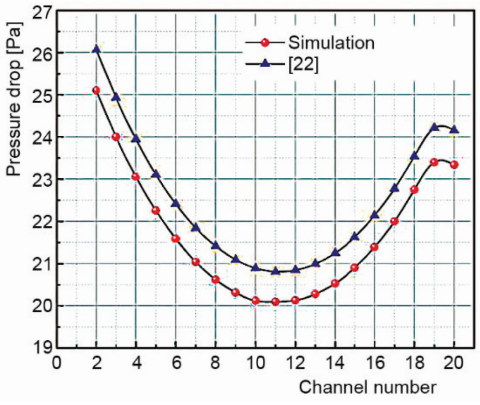

Figure 4. Verification of numerical simulation

where f is the Fanning friction factor, ΔP [Pa] – the pressure drop of the fully developed flow in the middle part of the micro-channel, and L – the length of the fully developed flow, L = 10 mm.

The results of pressure drop calculated by the CFD in the 20 micro-channels and this correlation have been presented in fig. 4. As can be seen, the difference between both results is generally less than 4%, which shows an excellent prediciton accuraccy for this numerical model. The data of Mohammadi *et al.* [22] is based on their experimental correlation in which the flow of water is uniform in each channel, while the numerical simulation results in this article considers the non-uniformity of the water flow in each channel,which may lead to the difference.

Optimization procedure

Design variables and objective function

In previous studies, the shape optimization of inlet header generally focused on the form of rectangle, trapezoid and triangle. For these shapes, the slanted edge of the inlet header is generally in the form of straight line. It lacks the ability to take local adjustments to the flow distribution in the inlet header. In this work, we just try to explore the effect of the parabolic slanted edge instead of the straight line for the inlet header on the flow distribution of the MCHS. Meanwhile, the flow rate V is also taken into consideration to study the effect of velocity on the flow mal-distribution. A plane Cartesian co-ordinate system is established in fig. 5. The point O is defined as the origin. The x-axis coincides with the bottom edge of the inlet header. The length of the bottom edge has been kept at x_1 = 4 mm. The top edge of the inlet header x_2 varied from 0 mm to 4 mm. A quadratic parabola is used instead of the original straight line for the slanted edge of the inlet header, and the slanted edge of the inlet header and the slanted edge of the outlet header are centrosymmetric in the article.In this case, the expression of the quadratic parabola can be defined:

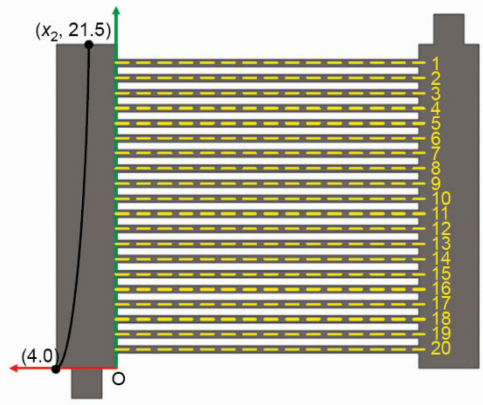

Figure 5. Diagram of plane Cartesian co-ordinate system in MCHS

$$y = a(x-b)(x-c) \tag{9}$$

where a, b, and c are the constant. Since the parabola passes through the both points (4,0) and (x_2, 21.5), eq. (10) can be written:

$$y = a(x-4)\left[x - x_2 + \frac{21.5}{a(x_2-4)}\right] \tag{10}$$

In this equation, the specific shape of the parabola can be determined once the parameters a and x_2 are known. The shape of the parabola is schematically shown in fig. 5. After testing, if the value of a is particularly large, it will in turn worsen the flow uniformity. Therefore, the value of a varies from –10 to 10 in this work. Meanwhile, six velocity conditions of 0.05 m/s, 0.06 m/s, 0.07 m/s, 0.08 m/s, 0.09 m/s, and 0.1 m/s were selected for the inlet to study the influence of flow rate.

To describe the flow uniformity in the micro-channel, the objective function of non-uniformity of fluid-flow is defined:

$$\varphi = \sqrt{\frac{1}{n}\sum_{i=1}^{n}\left(\frac{U_i}{\overline{U}} - 1\right)^2} \tag{11}$$

where U_i is the average velocity of the intermediate section of the i^{th} micro-channel and $\overline{U}$ – the mean velocity of all the micro-channels, n equals to 20.

Design of training samples and test samples

A surrogate model is necessary before searching for the optimal structure. Appropriate sampling of design points including parameters a and x_2 is required to construct the relationship between the parabola shape and the non-uniformity of fluid-flow using the Back propagation neural network (BPNN). Latin hypercube sampling (LHS) is an effective sampling method to make each point be equal space in the design space. The LHS uses a uniform sampling method to sample variables and then uses a random set of combinations of these variables in a single computation of the objective function [24]. The 40 design points are selected by the LHS in this study. Meanwhile, six design points are selected to verify the prediction model constructed by the surrogate model.

Surrogate model

The BPNN is a three layers network, which includes an input layer, a hidden layer and an output layer. The BPNN is widely used due to its simple structure, many adjustable parameters, rich training algorithms and good operability [25]. Figure 6 shows the structure of a general neuron model. The X_i means the input of the neuron i, ω_i means the connection weight of neuron i, θ is the thresholds, $f(x)$ is the output function that could be described:

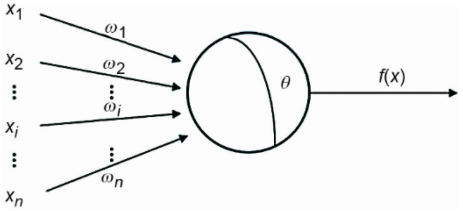

Figure 6. The structure of neuron model

$$f(x) = f\left(\sum_{i=1}^{n} X_i\omega_i - \theta\right) \tag{12}$$

Figure 7 shows the structure of BPNN network. In this model, each neuron receives input signals from other neurons. Each signal is passed through a weighted connection. The

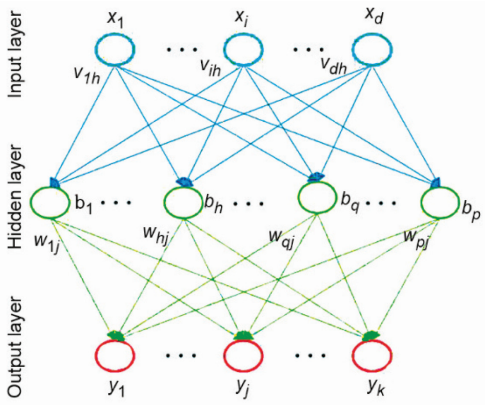

Figure 7. The structure of BPNN network

neuron adds these signals together to get a total input value. The total input value is compared to the threshold value of the neuron. The final output is processed through an activation function, which is then passed down as input from the subsequent neurons. In addition, the grid structure, the choice of initial connection weights and thresholds have a great impact on the training of BPNN. However, it is difficult to obtain the value accurately. Therefore, it is a key to determine the values of the BPNN for a specific case. In this paper, the GA is applied to optimize the initial connection weights and thresholds of the BPNN. This surrogate model that couples the GA and the BPNN can be defined as the GA-BP.

Optimization procedure

It is hard to construct a surrogate model and search for the optimal structure with conventional technique. The relationship between the parabola shape and the non-uniformity of fluid-flow is constructed by the GA-BP in the article. In the progress of optimization, the input variables of the GA-BP based on the sample data are the length of the upper line, x_2, the parabolic quadratic coefficient, a, and the velocity, V, of the inlet, and the objective function of non-uniformity of fluid-flow, φ, is the output variable. At the same time, φ is the objective function when optimizing the initial connection weights and thresholds of the BPNN by the GA. The GA is used to search for the optimal structure in the design space. The optimization process is shown in fig. 8. The selection function is set as the stochastic uniform function and the mutation function is set as the adaptive feasible function. The primary operation parameters of the GA-BP are listed in tab. 4.

Table 4. Primary parameters of GA-BP

Term	Value	Term	Value
Population size	120	Crossover probability	0.75
Maximum number of iterations	100	Mutation probability	0.01
Generation gap	0.95		

Result

In this study, 40 training sample points and six testing sample points are designed by the LHS. Thus, two samples containing 40 points and six points of different geometry structures can be generated with parabolic parameters a, x_2. The flow condition of each geometry structure is calculated by the CFD. Each point of geometry model should be calculated by the CFD for six different inlet velocities. According to the simulation results, the corresponding non-uniformity of 20 micro-channels φ can be obtained for every flow condition. To get the optimal structure for different flow rate of inlet, six surrogate models are separately trained with each one inlet velocity. Combined with the GA, six different optimal geometry structures can be obtained for every specify inlet velocity.

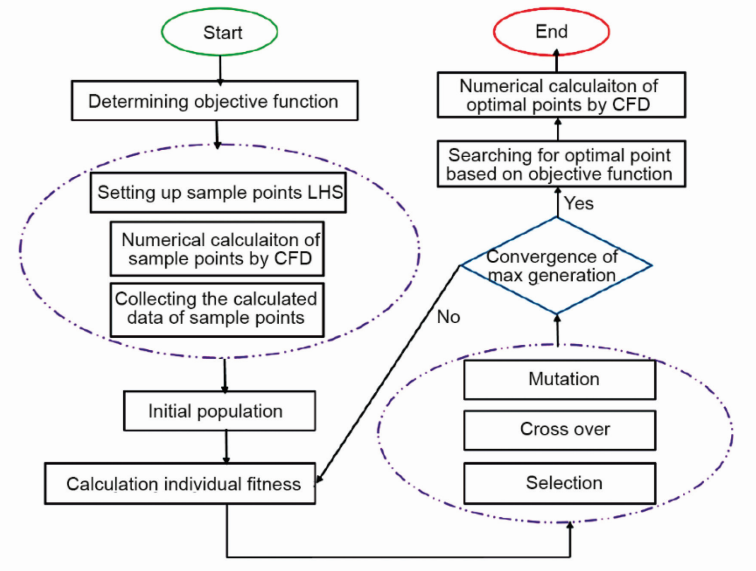

Figure 8. Flowchart of the entire GA-BP optimization

After analyzing, it is found that the parameters a and x_2 of the parabolic for the optimal structure is almost same for the working condition with small inlet velocity (0.05 m/s and 0.06 m/s). A similar condition occurred for the last four sets of velocities (0.07 m/s, 0.08 m/s, 0.09 m/s, and 0.10 m/s). As a matter of convenience, the optimized model obtained for the first two velocities is represented by the first group (0.05 m/s), and the optimized model obtained for the last four velocities is represented by the last group (0.10 m/s). Optimized design and its predicted value by the surrogate model and the actual value by the CFD of objective function at the optimized point are shown in tab. 5, which are better than 40 training sample points. In the six sets of the optimal structure obtained, the relative errors between the predicted and actual values of the objective function are within 7%, which ensures the prediction accuracy. Through the optimizations, the objective functions are reduced by 52.43%,

Table 5. Optimized design compared with original design for different inlet velocities

Term	x_2	a	V = 0.05 m/s			V = 0.06 m/s		
			Predicted φ	Actual φ	Error	Predicted φ	Actual φ	Error
Original design	4	–	–	0.0761	–	–	0.0722	–
Optimal structure	0.244	1.138	0.034	0.0362	6.47%	0.03	0.0413	5.6%
			V = 0.07 m/s			V = 0.08 m/s		
Original design	4	–	–	0.0761	–	–	0.0782	–
Optimal structure	0.824	-0.693	0.047	0.0441	6.58%	0.049	0.0467	4.69%
			V = 0.09 m/s			V = 0.10 m/s		
Original design	4	–	–	0.0788	–	–	0.0796	–
Optimal structure	0.824	-0.693	0.052	0.0493	5.19%	0.056	0.0532	5.00%

46.50%, 43.17%, 40.28%, 37.44%, and 33.17%, respectively, compared to those of the original design. The results show that the flow distribution of the MCHS can be greatly improved with the quadratic parabola line instead of straight line for the slanted edge of the inlet header.

At the same time, the flow resistance of the model is only slightly improved. Total pressure drop of original design and optimized design are shown in tab. 6. At an inlet velocity of 0.05 m/s, the total pressure drop only increased by 14.82% from an original 38.42 Pa to 44.13 Pa. For an inlet velocity of 0.10 m/s, this number is 9.57%. The change of total pressure drop mainly depends on the change of the friction pressure drop, which changes little with the velocity but greatly with the slanted edge of the MCHS. The increase of the pressure drop at 0.05 m/s is similar to the increase of the pressure drop at 0.1 m/s, while the total pressure drop at 0.05 m/s is much lower than that at 0.1 m/s, so the increase ratio of pressure drop at 0.05 m/s is higher than that at 0.1 m/s.

Table 6. Total pressure drop of original design and optimized design

Term	Velocity [ms^{-1}]	Original design	Optimized design	Increased by
Pressure drop [Pa]	$V = 0.05$	38.42	44.13	14.82%
	$V = 0.10$	76.45	83.77	9.57%

Figures 9 and 10 show the velocity field and streamline distributions on x-y plane (z = 0.25 mm) at the inlet velocity of 0.05 m/s for the original and optimized design, respectively. Similarly, figs. 11 and 12 show the flow condition at the inlet velocity of 0.10 m/s. The both optimal geometry structure models have a significant reduction of the separation zone in the inlet header. The slight difference is that at slower speeds, the concave shape of the header facilitates the uniformity of the flow distribution, while the convex shape of the header is more effective for a higher speed. The area of the header with the convex shape is larger than that of the header with the concave shape, so it is more effective to balance the kinetic energy distribution of the fluid. Streamline distributions indicate that the size and shape of the inlet separation zone has a significant influence on fluid-flow. The flow area in the original inlet header is larger, which is beneficial to reduce the entry effect. However, the distribution of the velocity field is not uniform. In the inlet header of the original structure, the velocity is relatively larger near the inlet or the outlet. At the other end of the inlet or outlet header, the velocity is relatively low. This indicates that the dynamic pressure in the vicinity of the inlet or outlet is large. According to the Bernouli's

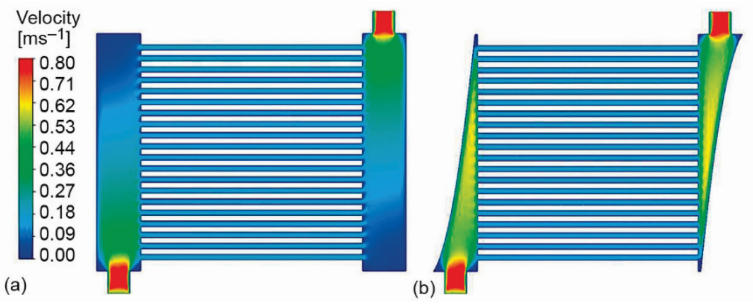

Figure 9. Velocity field of the original design (a) and optimized design (b) at the inlet velocity of 0.05 m/s

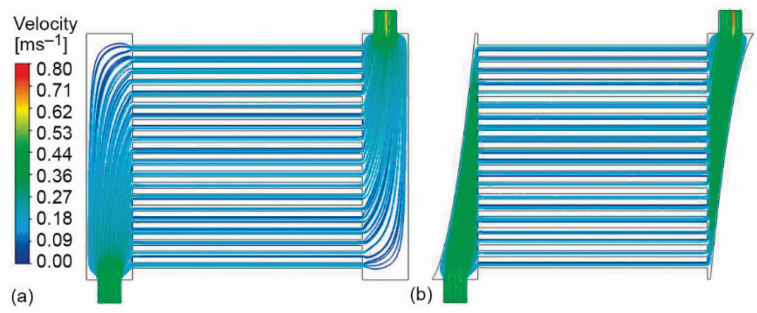

Figure 10. Streamlines of the original design (a) and optimized design (b) at the inlet velocity of 0.05 m/s

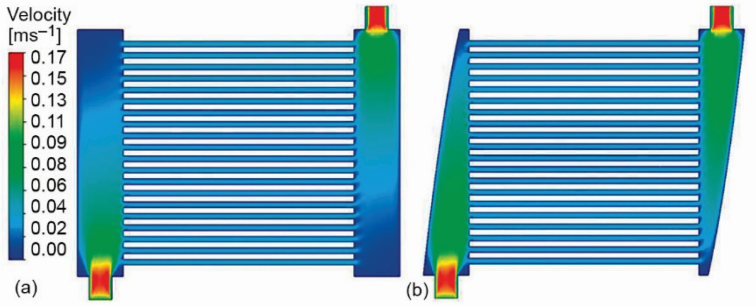

Figure 11. Velocity field of the original design (a) and optimized design (b) at the inlet velocity of 0.10 m/s

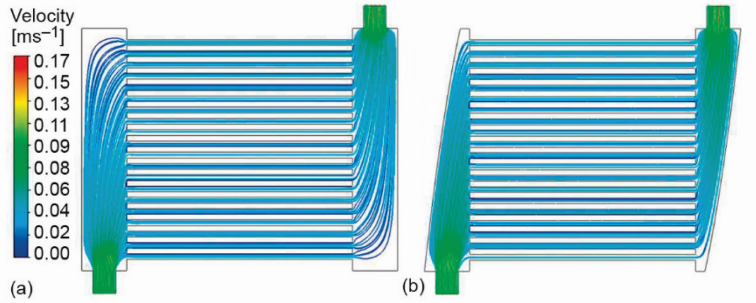

Figure 12. Streamlines of the original design (a) and the optimized design (b) at the inlet velocity of 0.10 m/s

law, the static pressure in these areas will be relatively small. The flow in the micro-channel is mainly driven by the pressure drop difference between the inlet and outlet headers. Therefore, the non-uniformity of the flow filed distribution in the inlet and outlet headers will lead to the non-uniformity of the flow rate in different micro-channels. By comparing the flow field distribution in the original structure and the optimal structure, it can be seen that the velocity field distribution in the inlet or outlet header is more uniform for the optimal structure, especially under the condition of low flow rate.

To demonstrate the relative flow distribution of channels, normalized dimensionless velocity is defined:

$$U_i' = \frac{U_i}{\overline{U}} \tag{13}$$

The closer the U_i is to 1, the smaller the deviation of the outlet velocity of the i^{th} micro-channel to the average outlet velocity of the all micro-channels. Figure 13 shows the normalized velocity of the original design and optimized design at two different inlet velocities. The optimized designs have a more uniform flow distribution, especially for the micro-channels located in the central part. It also indicates that the optimization effect at low flow rate is better than that at high flow rate, which may be related to the reduced weight of the effect of the header shape on the flow distribution at high flow rate.

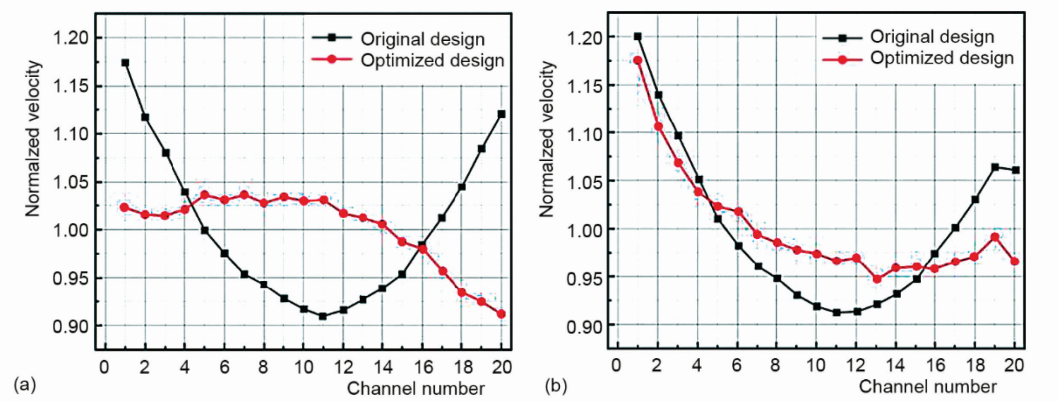

Figure 13. Normalized velocity of the original design and optimized design, at the inlet velocity of 0.05 m/s (a) and 0.10 m/s (b)

Conclusions

In present work, the fluid-flow uniformity of a MCHS is improved by the means of optimizing the slanted edge with the quadratic parabola for the inlet header. The 40 training sample points and six testing sample points are designed by the LHS method. The GA-BP is used as the surrogate model to predict the fluid-flow distribution with different designed parameters of the MCHS. The GA is applied to obtain the optimal parameters. The objective function is defined as the non-uniformity of the fluid-flow for all the micro-channels. Through the optimizations, the non-uniformity of the MCHS are reduced by 52.43%, 46.50%, 43.17%, 40.28%, 37.44%, and 33.17% at the inlet velocity of 0.05 m/s, 0.06 m/s, 0.07 m/s, 0.08 m/s, 0.09 m/s, and 0.10 m/s, respectively, compared to those of the original design. The optimized designs have a more uniform flow distribution, especially under the condition of low flow rate. Meanwhile, a slight increase in the total pressure drop of the MCHS is found, which is acceptable. By appropriately reducing the separation zone and matching the appropriate quadratic parabola of the slanted edge for the inlet header to the inlet velocity, the flow in the section of the inlet header can be deflected, thereby promoting the uniformity of the flow distribution in the micro-channels.

Acknowledgment

This research was funded by the National Key R&D Program of China (grant number: 2022YFB4100801), which are gratefully acknowledged.

References

[1] Zhu, Q, *et al*., Effects of Geometric Parameters on Fluid-flow and Heat Transfer in Micro-channel Heat Sink with Trapezoidal Grooves in Sidewalls, *Thermal Science*, *26* (2022), 4B, pp. 3641-3651
[2] Choong, J. Y., *et al.,* Numerical Assessment on Heat Transfer Performance of Double-Layered Oblique Fins Micro-Channel Heat Sink with Al_2O_3 Nanofluid, *Thermal Science*, *26* (2022), 1B, pp. 477-488
[3] Wen, J., *et al*., Optimization Investigation on Configuration Parameters of Serrated Fin in Plate-Fin Heat Exchanger Using Genetic Algorithm, *International Journal of Thermal Sciences*, *101* (2016), Mar., pp. 116-125
[4] Anbumeenakshi, C., Thansekhar, M. R., On the Effectiveness of a Nanofluid Cooled Microchannel Heat Sink Under Non-uniform Heating Condition, *Applied Thermal Engineering, 113* (2017), Feb., pp. 1437-1443
[5] Tuckerman, D. B., Pease, R. F. W., High-Performance Heat Sinking For VLSI, *Electron Device Letters, 2* (1981), 5, pp. 126-129
[6] Dewan, A., *et al.,* Review of Passive Heat Transfer Augmentation Techniques, Proc. Inst. Mech. Eng. Part A-*J. Power Energy, 218* (2004), 7, pp. 509-527
[7] Bajura, R. A., Jones, E. H., Flow Distribution Manifolds, *J. Fluids Eng-Trans. ASME, 98* (1976), 4, pp. 654-666
[8] Arie, M. A. *et al.,* Numerical Modeling and Thermal Optimization of a Single-Phase Flow Manifold-Micro-channel Plate Heat Exchanger, *Int. J. Heat Mass. Tran., 81* (2015), Feb., pp. 478-489
[9] Jackson, J. M., *et al.,* Discrete Geometry Optimization for Reducing Flow Non-Uniformity, Asymmetry, and Parasitic Minor Loss Pressure Drops in Z-Type Configurations Of Fuel Cells, *Journal of Power Sources, 269* (2014), Dec., pp. 274-283
[10] Midoux, N., Tondeur, D., The Theory of Parallel Channels Manifolds (Ladder Networks) Revisited Part 1: Discrete Mesoscopic Modelling, *Canadian Journal of Chemical Engineering, 92* (2014), 10, pp. 1798-1821
[11] Pan, M. Q., *et al.,* Numerical Simulation of the Fluid-flow and Heat Transfer Characteristics of Micro-channel Heat Exchangers with Different Reentrant Cavities, *Int. J. Numer Methods Heat Fluid-flow, 29* (2019), 11, pp. 4334-4348
[12] Solovitz, S. A., Mainka, J., Manifold Design for Micro-Channel Cooling with Uniform Flow Distribution*, Journal of Fluids Engineering, 133* (2011), 5, 051103
[13] Manikanda Kumaran, R., *et al.,* Experimental and Numerical Studies of Header Design and Inlet/Outlet Configurations on Flow Mal-Distribution in Parallel Micro-Channels, *Applied Thermal Engineering, 58* (2013), 1-2, pp. 205-216
[14] Sehgal, S. S., *et al.,* Effect of Channel and Plenum Aspect Ratios on the Performance of Micro-channel Heat Sink Under Different Flow Arrangements*, Journal of Mechanical Science and Technology, 26* (2012), Sept., pp. 2985-2994
[15] Koo, G.-W., *et al.,* Shape Optimization of Inlet Part of a Printed Circuit Heat Exchanger Using Surrogate Modeling*, Applied Thermal Engineering, 72* (2014), 1, pp. 90-96
[16] Shi, H.-N., *et al.,* Optimization of Inlet Part of a Micro-channel Ceramic Heat Exchanger Using Surrogate Model Coupled with Genetic Algorithm, *Energy Conversion and Management, 149* (2017), Oct., pp. 988-996
[17] Wen, J., *et al.,* Configuration Parameters Design and Optimization for Plate-Fin Heat Exchangers with Serrated Fin by Multi-Objective Genetic Algorithm, *Energy Conversion and Management, 117* (2016), June, pp. 482-489
[18] Yang, Y., *et al*., Optimizing the Size of a Printed Circuit Heat Exchanger by Multi-Objective Genetic Algorithm, *Applied Thermal Engineering, 167* (2020), Feb., 114811
[19] Alperen, Y., Sertac, C., Multi Objective Optimization of a Micro-Channel Heat Sink Through Genetic Algorithm, *Int. J. Heat Mass. Tran., 146* (2020), Jan., 118847
[20] Ge, Y., *et al.,* Optimal Shape Design of a Minichannel Heat Sink Applying Multi-Objective Optimization Algorithm and Three-Dimensional Numerical Method, *Applied Thermal Engineering, 148* (2019), Feb., pp. 120-128

[21] Wang, T.-H., *et al.,* Optimization of a Double-Layered Micro-Channel Heat Sink with Semi-Porous-Ribs by Multi-Objective Genetic Algorithm, *Int. J. Heat Mass. Tran., 149* (2020), 119217
[22] Mohammadi, M, *et al.,* Numerical study of flow uniformity and pressure characteristics within a micro-channel array with triangular manifolds, *Computers & Chemical Engineering*, *52* (2013), May, pp. 134-144
[23] Shah, R. K., London, A. L., *Laminar Flow Forced Convection in Ducts*, Academic Press, New York, 1978
[24] Dong, F., *et al*., Numerical Study on Flow and Heat Transfer Performance of Serpentine Parallel Flow Channels in A High Voltage Heater System, *Thermal Science, 26* (2022), 1B, pp. 735-752
[25] Jiang, M., Pan, Z, Optimization of Micro-Channel Heat Sink with Trapezoidal Cavities and Solid/Slotted Oval Pins Based on Genetic Algorithm and Back Propagation Neural Network, *Thermal Science, 27* (2023), 1A, pp. 179-193

Paper submitted: December 19, 2022
Paper revised: February 15, 2023
Paper accepted: March 6, 2023